Engineering

Electrical Engineering fields

Okayama University *Year* 2000

Analysis and reduction of EMI conducted by a PWM inverter-fed AC motor drive system having long power cables

Satoshi Ogasawara
Okayama University

Hirofumi Akagi
Tokyo Institute of Technology

Analysis and Reduction of EMI Conducted by a PWM Inverter-Fed AC Motor Drive System Having Long Power Cables

Satoshi Ogasawara* and Hirofumi Akagi**
*Department of Electrical Engineering, Okayama University
3-1-1 Tsushima-naka, Okayama, 700-8530 JAPAN
**Department of Electrical Engineering, Tokyo Institute of Technology
2-12-1 O-okayama, Meguro, Tokyo, 152-8552 JAPAN

Abstract— **This paper analyzes conducted EMI generated by a PWM inverter-fed induction motor drive system. It is shown experimentally and analytically that resonant phenomena in a high-frequency range beyond a dominant resonant frequency are originated from the behavior of power cables as a distributed-constant circuit. Spectra of common-mode and differential-mode currents are simulated by means of introducing a distributed-constant model of the power cables, which consists of a 20-step ladder circuit. As a result, it is also shown that these resonances can be damped out by a single common-mode transformer (CMT) and three differential-mode filters (DMF's), both of which have been proposed by the authors.**

I. Introduction

In recent years, development of high-speed power semiconductor devices has brought high-frequency switching operation to power electronic equipment and has improved performance of pulsewidth-modulated (PWM) inverters for driving ac motors. However, electromagnetic interference (EMI) has been pointed out as a serious problem [1]–[5]. A steep change in voltage and/or current caused by high-speed switching operation produces high-frequency oscillatory common-mode and differential-mode currents because of parasitic stray components inevitably existing in an ac drive system. The oscillatory currents can create EMI noises throughout, thus producing a bad effect on electronic devices such an AM radio receiver and medical equipment.

The authors have proposed an equivalent circuit that can simulate both common-mode and differential-mode currents at the same time [6]. Here, the common-mode current is a high-frequency oscillatory current escaping through stray capacitors between motor windings and a frame to a grounding conductor. On the other hand, the differential-mode current is a high-frequency oscillatory current flowing among the three phases. The already proposed equivalent circuit consisting of lumped-constant elements can simulate dominant resonances of the common-mode and differential-mode currents. In addition, the authors have proposed a common-mode transformer (CMT) and a differential-mode filter (DMF), and experimental results have confirmed their effectiveness in damping of high-frequency oscillatory currents [7].

This paper analyzes conducted EMI generated by a PWM inverter-fed induction motor drive system. Some experimental results show that the spectrum of the conducted EMI has several peaks in a high-frequency range beyond the dominant resonant frequency. It is analyzed that these resonant phenomena in the high-frequency range originate from the behavior of the power cables as a distributed-constant circuit. A distributed-constant model of the power cables, which consists of a 20-step ladder circuit, is introduced to simulate spectra of the common-mode and differential-mode currents using a circuit simulator (PSpice). As a result, it is shown experimentally and theoretically that the common-mode transformer (CMT) and the differential-mode filters (DMF's) can damp out these resonances.

II. System Configuration

Fig. 1 shows the configuration of an experimental system in which an IGBT inverter feeds an induction motor rated at 3.7 kW. The inverter is equipped with the so-called sinusoidal PWM scheme based on comparing three-phase sinusoidal waves with a triangular wave having a frequency of 10 kHz. Output terminals of the inverter are connected to input terminals of the induction motor through three-phase power cables (conductor sectional area: 5.5 mm^2, length: 10 m), and the motor frame is connected to virtual ground through a grounding conductor (5.5 mm^2, 10 m).

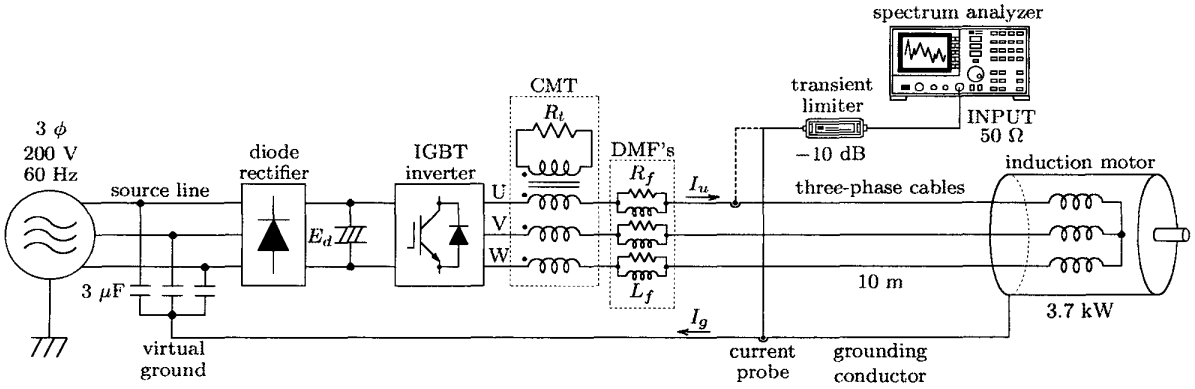

Fig. 1. System configuration.

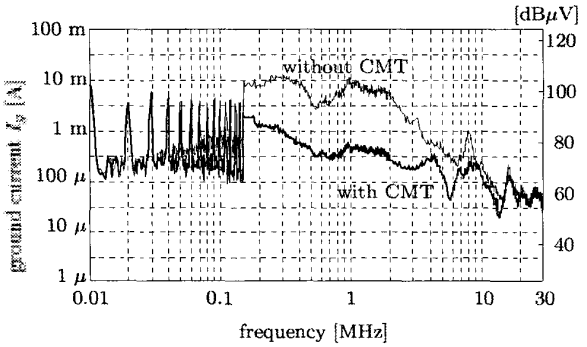

Fig. 2. Experimental spectra of ground current.

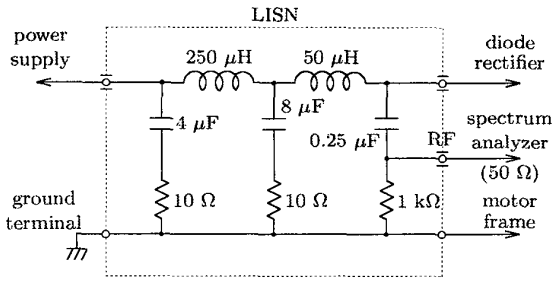

Fig. 3. Per-phase circuit of LISN.

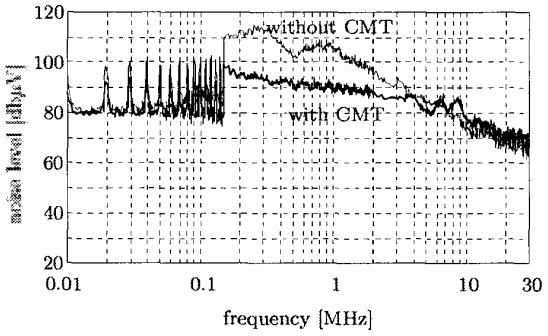

Fig. 4. Experimental spectra of conducted EMI.

This virtual ground is a neutral point of Y-connected capacitors that are connected to input terminals of a diode rectifier, and it is intended to avoid the influence of an internal impedance behind the switchboard [6].

A common-mode transformer (CMT) and three differential-mode filters (DMF's) are attached to the ac output side of the inverter. The CMT is the same as the common-mode choke except for having an additional isolated winding, the terminals of which are shorted by a resistor. The CMT can damp out oscillation of the common-mode current, i.e., high-frequency leakage or ground current flowing through the grounding conductor [6]. Each DMF acts as a resistor in a high-frequency range, although it acts as a small inductor in a low-frequency range. Hence, a set of three DMF's can damp high-frequency oscillation of differential-mode currents which flow among three-phase power cables at every switching of the IGBT's [7]. Measurement of a current spectrum is performed using a current prove (Tektronix AM503, A6303), a limiter (HP 11947A) and a spectrum analyzer (HP 8590L). In order to evaluate both common-mode and differential-mode currents, the ground current I_g and u-phase current I_u are measured.

III. Measurement of Current Spectrum

A. Common-mode current

Fig. 2 shows a spectrum of the ground current I_g, i.e., the common-mode current. In a frequency range from 10 kHz to 150 kHz, a sequence of impulse spectra appears at intervals of the switching frequency of 10 kHz, where the spectrum analyzer used for measurement has a resolution bandwidth of 200 Hz. In a frequency range beyond 150 kHz, I_g looks like a continuous spectrum, because the resolution bandwidth is switched to 9 kHz. When no CMT is installed, the spectrum decreases by -40 dB/dec in a frequency range beyond 1 MHz. However, several peaks exist at 8 MHz and 16 MHz, and so on. For the common-mode current, an equivalent circuit proposed in [6] is represented as a resonant circuit that consists of lumped line inductors and stray capacitors. The equivalent circuit (hereafter referred to as the lumped-constant model) can not explain why the peaks appear in such a high-frequency range, although it is valid enough for the dominant common-mode current in a frequency range up to 3 MHz. In order to analyze such a phenomenon, it is necessary to introduce a new analytic model.

Fig. 2 also shows the spectrum in the case with the CMT. The common-mode current is reduced not only around 1 MHz but also in the high-frequency range. This experimental result shows that the CMT is capable of reducing the common-mode current both in the vicinity of the dominant resonant frequency around 1 MHz and in the high-frequency range.

Moreover, conducted EMI in a frequency range between 10 kHz and 30 MHz is measured to investigate a relationship to the common-mode current, by using a line impedance stabilization network (LISN: Kyouritsu KNW-243C) connected between the power supply and rectifier input terminals. Fig.3 shows an inside circuit per phase of the LISN. Since a spectrum analyzer having an input impedance of 50 Ω is connected to the RF output terminal, almost all the common-mode current distributed to each phase flows through the 0.25-μF capacitor. The conducted EMI is measured as a voltage across the 50-Ω resistor flowing 1/3 of the common-mode current, because the circuit shown in Fig. 3 is connected in parallel with each phase. For example, a common-mode current of 10 mA is converted to its corresponding conducted EMI as follows:

$$20\log\frac{50\,\Omega\times 10\,\mathrm{mA}\times(1/3)}{1\,\mu\mathrm{V}} = 104\,\mathrm{dB}\mu\mathrm{V}. \qquad (1)$$

Graduations with a unit of dBμV are put together on the right side of Fig. 2.

Fig. 4 shows a measured spectrum of the conducted EMI. Since Fig. 4 is similar to Fig. 2, it is obvious that the common-mode current has a strong relationship with the conducted EMI, although the resistor of 50 Ω acts as a damping resistor for the common-mode current.

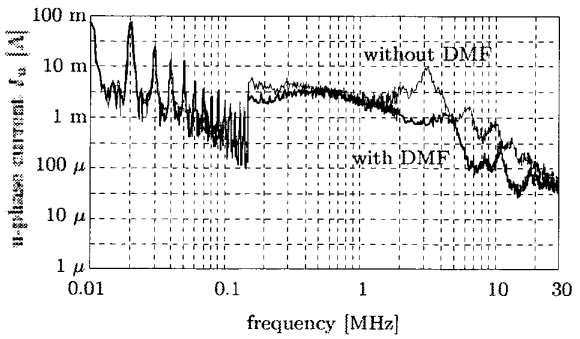

Fig. 5. Experimental spectra of phase current.

B. Differential-mode current

Fig. 5 shows a spectrum of the u-phase current I_u. The differential-mode current flows in the u-phase power cable, along with 1/3 of the common-mode current. Similar to the common-mode current, the spectrum of I_u has several peaks in a frequency range higher than a dominant resonant frequency of 3 MHz which can be represented by a conventional lumped model. In a high-frequency range over 5 MHz, the spectrum of Fig. 5 has resonant phenomena.

Moreover, it is shown that the u-phase current decreases not only around the dominant resonant frequency but also in a higher-frequency range when the DMF's are connected.

IV. Distribution-Constant Model of Power Cables

In a frequency range above 5 MHz in Figs. 2 and 5, there exist resonant phenomena, which can not be explained by the lumped-constant model. The following discusses a distributed-constant model of power cables to evaluate the resonant phenomena in this frequency range.

A. Frequency characteristics of power cables

In order to investigate the resonant phenomena of power cables, frequency characteristics of the ground current I_g and the phase current I_u are measured in a circuit configuration shown in Fig. 6. A tracking generator integrated into a spectrum analyzer is connected with the power cables at the inverter-side terminals, and it generates a sinusoidal voltage of 1 V. Three capacitors emulating stray capacitors between motor windings and a motor frame are connected to the motor-side terminals. A current probe measures the ground and phase currents. Fig. 6 assumes that a switching occurs in u-phase of the three-phase inverter while the other phases are closed on the negative side of the dc link.

Figs. 7 and 8 show frequency characteristics of I_g and I_u, in which I_g falls in resonance at 1.3 MHz, and I_u has a resonance at about 2.5 MHz, which is twice the resonant frequency of I_g. The two resonant frequencies agree with those calculated from the lumped-constant model. However, several resonances exist at every frequency interval of 8 MHz, e.g., at 8, 16 and 24 MHz. These resonant frequencies coincide with those in Figs. 2 and 5. Therefore, the power cables should be regarded as a distributed-constant circuit for analysis in a frequency range higher than 5 MHz.

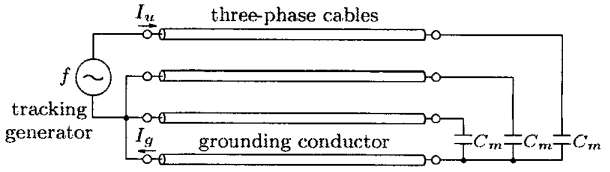

Fig. 6. Measurement for frequency characteristics of power cables.

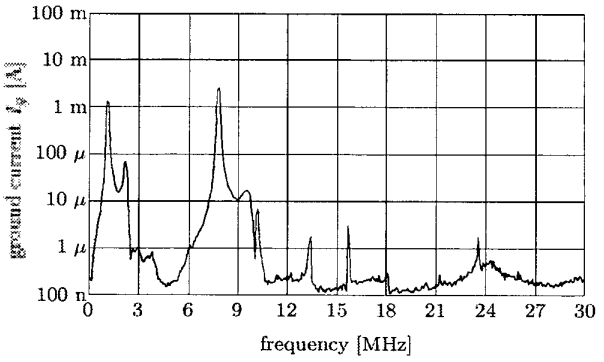

Fig. 7. Frequency characteristics of I_g.

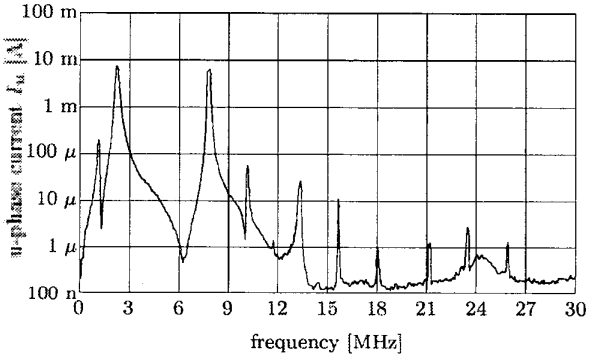

Fig. 8. Frequency characteristics of I_u.

It is necessary to consider a frequency bandwidth for analysis and a cable length when the power cables are treated as a distributed circuit. The frequency bandwidth can be determined from the rise time of the inverter output voltage or the frequency range for measurement. Here, the frequency bandwidth is decided as 30 MHz from the frequency range of the conducted EMI measurement. The power cables exhibit phenomena as a distributed circuit, when the cable length is longer than 1/4 of the wavelength, i.e., 2.5 m.

B. Measurement of Cable Parameters

Cable parameters as a distributed-constant circuit are measured by using an LCR meter (HP 4263A). The measuring frequency is 100 kHz, which is much lower than the first resonant frequency of the distributed-constant circuit. As shown in Fig. 9, the motor-side terminals are shorted in case of measurement of the line inductance and resistance. Conversely, the motor-side terminals are opened for measuring the line capacitance. Table I shows the measured

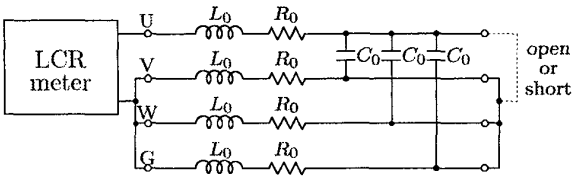

Fig. 9. Measurement of circuit constants using an LCR meter.

TABLE I
CIRCUIT PARAMETERS OF POWER CABLES.

inductance L_0 [μH]	resistance R_0 [mΩ]	capacitance C_0 [pF]
3.9	176.7	227.5

circuit parameters of the power cables. Here, L_0 and R_0 mean the inductance and resistance existing in one power cable or ground conductor, and C_0 means the capacitance between two cables, as shown in Fig. 9.

C. Distributed-Constant Model

A distributed-constant model consisting of an n-step ladder circuit shown in Fig. 10 is introduced, in order to evaluate the power cables as a distributed-constant circuit by using a circuit simulator such as SPICE. Each value of the circuit element is given as the corresponding measured value divided by the step number n. However, n has a significant influence on the simulation accuracy. Considerations on the optimal step number will be described in detail below.

A distributed-constant circuit has a resonant frequency f_1, at which the cable length is equal to 1/4 of the wavelength. Moreover, the distributed-constant circuit causes resonant phenomena at intervals of f_1. Assuming the bandwidth to be B, the number of the resonances in the bandwidth is given by B/f_1. On the other hand, the distributed-constant model consisting of the n-step ladder circuit has

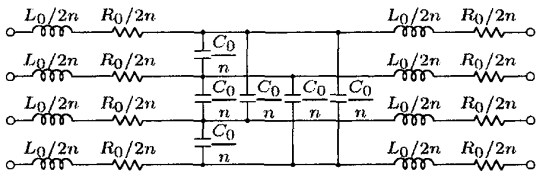

Fig. 10. Distributed-constant model per step for power cables.

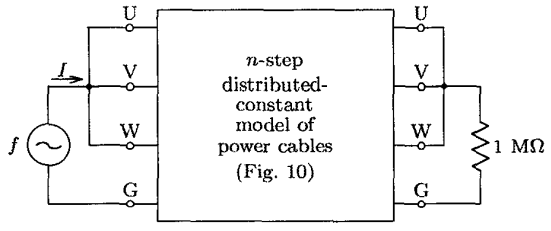

Fig. 11. Simulated model to determine the optimal step number.

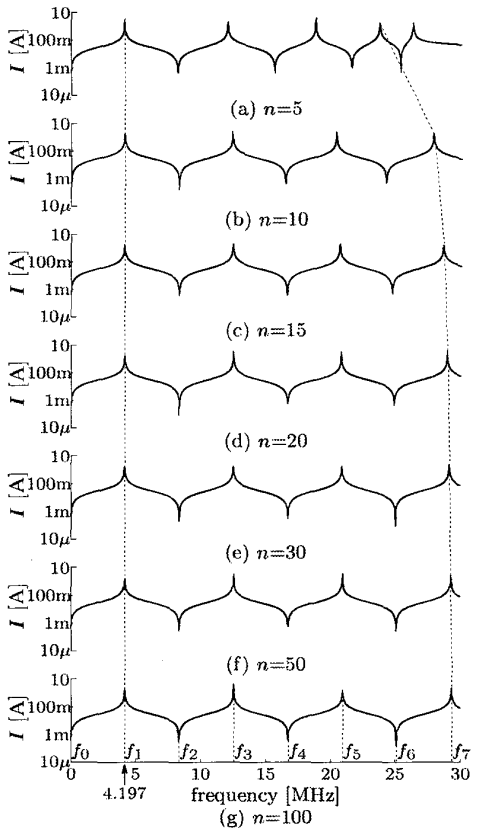

Fig. 12. Difference in frequency characteristics with respect to n.

$2n$ resonant frequencies. The minimum step number N, therefore, is given by

$$N > \frac{B}{2f_1}. \tag{2}$$

In this case, since $B = 30$ MHz and $f_1 = 4.197$ MHz, n should be selected to a number greater than 4. In terms of accuracy of the resonant frequency, n is a number much larger than 4. However, as n is selected to be larger, the execution time for simulation becomes longer.

Fig. 11 shows a simulation model to determine the optimal step number, using "ac analysis" available in PSpice. A voltage source of 1 V is connected to the inverter-side terminals, while a resistor of 1 MΩ is connected to the motor-side terminals to prevent the terminals from floating nodes. Since the resistance is much larger than the characteristic impedance, the terminals are almost opened. Theoretically, the resonances appear at even frequency intervals of f_1.

Fig. 12 shows differences in the frequency characteristics with respect to n. In the case of a small number, a large amount of frequency error occurs in a higher-frequency range. Since the bandwidth is 30 MHz, the frequency characteristics should be simulated up to the 7th resonant frequency with good accuracy. The theoretical frequency of the 7th resonance is

$$f_{7t} = 7f_1 = 29.38 \quad [\text{MHz}]. \tag{3}$$

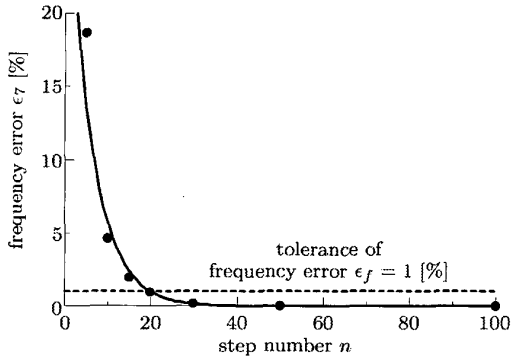

Fig. 13. Simulation result of relationship between ϵ_7 and n.

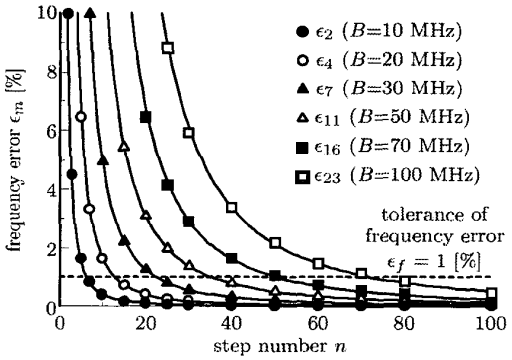

Fig. 14. Analytical result of relationship between ϵ_m and n .

An error with respect to the m-th resonant frequency is defined as

$$\epsilon_m = \frac{f_{mt} - f_m}{f_{mt}} \times 100 \quad [\%]. \tag{4}$$

Fig. 13 shows a relationship between the frequency error ϵ_7 and the step number n. As the step number n increases from 20, the 7th error decreases to 1 % or less and finally reaches zero. Therefore, the optimal step number can be selected as 20, under the condition of a frequency error less than 1 %.

Since both bandwidth and cable length influence frequency error as mentioned above, the optimal step number n_o is not always 20 under other conditions. For the purpose of selecting the optimal step number under any condition, an analysis of the frequency error has been performed using Mathematica.

Fig. 14 shows an analytical result of resonant-frequency errors, when the bandwidth B is changed from 10 MHz to 100 MHz. The frequency errors are indicated in the highest-order resonance corresponding to the bandwidth. The following relationship exists between the optimal step number per wavelength k and the resonant order m, because the cable length is equal to $m/4$ times the wavelength.

$$k = \frac{4n_o}{m} \tag{5}$$

For example, in the cases of B = 10 MHz or 100 MHz, the optimal step number of 6 or 71 is obtained from Fig. 14, assuming the tolerance of the frequency error ϵ_f to be 1 %. The optimal step number per wavelength is calculated as 12 or 12.35, respectively. This result shows that the optimal step number per wavelength is always constant in any condition. The same result can be obtained even though the tolerance of the frequency error ϵ_f is changed. Table II shows the relationship between ϵ_f and k. When the bandwidth B, the cable length ℓ and the frequency tolerance ϵ_f are determined, Table II gives us the optimal step number per wavelength k. Under the experimental conditions in Figs. 2 and 5, the optimal step number n_o is determined simply as follows:

$$n_o = k\frac{m}{4} = 12 \times \frac{7}{4} = 21. \tag{6}$$

TABLE II
OPTIMAL STEP NUMBER PER WAVELENGTH.

ϵ_f [%]	1	2	3	5	7	10
k	12	9	7	6	5	4

V. SIMULATION USING DISTRIBUTED-CONSTANT MODEL

A. Simulation model

Fig. 15 shows a distributed-constant model for simulation of the motor drive system. The voltage-source inverter is represented by a pulse voltage source, the amplitude of which is equal to the dc-link voltage E_d. It is assumed that u-phase switches to the positive side when all phases are closed on the negative side. Here, the rise time is set to 150 ns from measurement of the output voltage. Since the CMT acts only to common-mode, it is represented by an LR parallel circuit in the grounding circuit. R_t and L_t simulate a damping resistor connected to the secondary winding and a magnetizing inductance of the transformer,

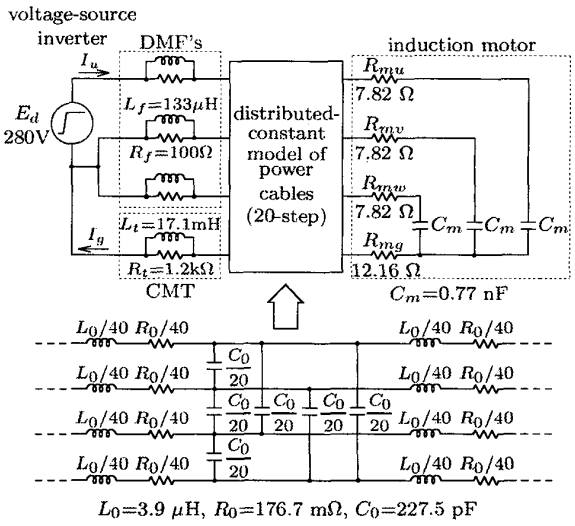

Fig. 15. Distributed-constant model for the motor drive system.

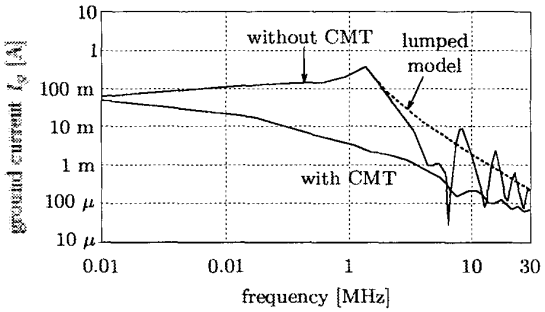

Fig. 16. Simulated spectra of ground current.

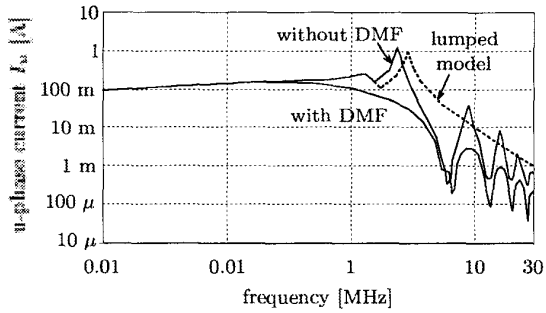

Fig. 17. Simulated spectra of phase current.

respectively. Another LR parallel circuit inserted between the inverter and the power cable represents the DMF.

In this analysis, transient current waveforms are simulated for 10 μs, and the spectra are calculated by means of FFT. Since the switching frequency of the inverter is 10 kHz (period 100 μs), the amplitude of the simulated spectrum is about 10 times (20 dB) as large as that of the experimental spectrum.

B. Spectrum of common-mode current

Fig. 16 shows simulated spectra of ground current I_g by applying the distributed model when the CMT is connected or not. Note that a dotted line shows a simulated spectrum by applying the lumped model in the case of no CMT. In a high-frequency range over 2 MHz, the spectrum of the distributed model has several peaks, compared with that of the lumped model. Furthermore, the peak frequencies simulated by applying the distributed model coincide with the experimental results shown in Fig. 2. This fact indicates that the behavior of the power cables as a distributed-constant circuit causes the peaks at 8 MHz and 16 MHz in the common-mode current spectrum. On the other hand, the simulated result of I_g shows that the CMT has a good effect on damping of not only the dominant resonance that can be represented by the lumped model, but also the peaks caused by the distributed-constant phenomena.

C. Spectrum of differential-mode current

Fig. 17 shows a simulated spectrum of u-phase current I_u. In the case of no DMF, a difference in dominant resonant frequencies of about 2 MHz exists between the spectra of the distributed model and the lumped model. The reason for this is that capacitances existing among the three power cables and the grounding conductor are neglected in the lumped model. Except for the frequency difference between the dotted line and the solid line without DMF in Fig. 17, the two spectra are almost the same below the dominant resonant frequency. The distributed model can simulate the resonant phenomena in a high-frequency range, whereas the lumped model can not do it, judging from Fig. 5. When the three DMF's are connected, the resonance at 2.4 MHz can be damped almost perfectly and almost no resonance phenomena occur in the high-frequency range.

VI. Conclusions

This paper has analyzed spectra of ground and phase currents, which contribute to conducted EMI in a PWM inverter-fed induction motor drive system. The analysis and simulation using a distributed-constant model of power cables have concluded as follows:

- Resonant phenomena in a frequency range higher than 5 MHz are caused by the behavior of the power cables as a distributed-constant circuit.
- The distributed-constant model composed of an n-step ladder circuit makes it possible to simulate the resonances in the high-frequency range.
- The optimal step number per wavelength in the distributed model is invariable, irrespective of the analysis bandwidth or cable length.

Experiments using an induction motor drive system rated at 3.7 kW have confirmed the validity and effectiveness of the distributed model. Furthermore, simulated and experimental results have shown the effect of the CMT and DMF's on mitigating the resonances in a higher-frequency range. Since the distributed model discussed in this paper is available in most of circuit simulators used for power electronics circuits, the use of the model is an effective way to analyze spectra of conducted EMI.

References

[1] Y. Murai, T. Kubota, and Y. Kawase: "Leakage Current Reduction for a High-Frequency Carrier Inverter Feeding an Induction Motor," *IEEE Trans. Industry Applications*, vol. 28, no. 4, pp.858–863, Jul./Aug., 1992.

[2] E. Zhong and T. A. Lipo: "Improvement in EMC Performance of Inverter-Fed Motor Drives," *IEEE Trans. Industry Applications*, vol. 31, no. 6, pp. 1247–1256, 1995.

[3] A. von Jouanne, P. N. Enjeti, and W. G. Gray: "Application issues for PWM Adjustable Speed AC Motor Drives," *IEEE Industry Applications Magazine*, vol. 2, no. 5, pp. 10–18, Sep./Oct. 1996.

[4] L. Ran, S. Gokani, J. Clare, k. J. Bradley, and C. Christopoulos: " Conducted Electromagnetic Emission in Induction Motor Drive Systems Part II: Frequency Domain Models," *IEEE Trans. Power Electronics*, vpl. 13, No. 4, pp. 768–776, July 1998.

[5] G. L. Skibinski, R. J. Kerkman, and D. Schlegel: "EMI Emissions of Modern PWM ac Drives," *IEEE Industry Applications Magazine*, vol. 5, no. 6, pp. 47–81, Nov./Dec. 1999.

[6] S. Ogasawara and H. Akagi: "Modeling and Damping of High-Frequency Leakage Currents in PWM Inverter-Fed AC Motor Drive Systems," *IEEE Trans. Industry Applications*, vol. 32, no. 5, pp. 1105–1114, 1996.

[7] S. Ogasawara, H. Ayano, and H. Akagi: "Measurement and Reduction of EMI Radiated by a PWM Inverter-Fed AC Motor Drive System," *IEEE Trans. Industry Applications*, vol. 33, No. 4, pp. 1019–1026, Jul./Aug., 1997.